Flow Visualization and Forces From a Squeeze Film
Damper Operating With Natural Air Entrainment

by

Dr. Luis San Andrés

May 2001

TRC-SFD-1-01

FLOW VISUALIZATION AND FORCES FROM A SQUEEZE FILM DAMPER OPERATING WITH NATURAL AIR ENTRAINMENT

Luis San Andrés, Professor

EXECUTIVE SUMMARY

Squeeze film dampers (*SFDs*) are effective means for force isolation and vibration attenuation in rotating machinery. However, *SFD* design remains empirical since predictive models fail to account for the complex effects of air ingestion; most persistent in operation with low levels of feed pressure and high whirl speeds. High performance - light weight turbomachinery favors these operating conditions.

Research at TAMU continues to advance the understanding of the flow mechanics in *SFDs*. Presently, measurements of dynamic film pressures and high-speed photographs of the flow field in a *SFD* operating with natural free air entrainment are forwarded. The experiments were conducted in a constrained orbit, open-ended *SFD* for increasing whirl frequencies ($\omega \rightarrow$ 8.33-50 Hz), and a range of feed pressures to 250 kPa (37 psig); thus spanning flow conditions from lubricant starvation (air ingestion) to a fully flooded discharge condition.

The test dynamic pressures and video recordings show that air entrainment leads to large and irregular gas fingering and striation patterns. This is a natural phenomenon in *SFDs* operating with low levels of external pressurization (low lubricant through flow rates). Air ingestion and entrapment becomes more prevalent as the whirl frequency raises, and increasing the feed pressure aids little to ameliorate the loss in dynamic forced performance. Estimated *SFD* damping forces decrease steadily as the whirl frequency (operating speed) increases, in direct opposition to Classical Lubrication predictions, and as a result of the severity of air entrainment.

The observations and correlations presented are not conclusive since the lubricant did not maintain a uniform temperature (viscosity) over the long test time that spanned the range from low to high feed pressures. More experiments without this unforeseen characteristic are planned to further the current understanding of *SFD* performance.

Digital movies of the recorded flow field, journal motion and pressure measurements may be downloaded from http://metrib.tamu.edu/SFDmovies.

FLOW VISUALIZATION AND FORCES FROM A SQUEEZE FILM DAMPER OPERATING WITH
NATURAL AIR ENTRAINMENT

TABLE OF CONTENTS

NOMENCLATURE

C	SFD nominal radial clearance [0.254 mm].
D	Journal diameter [129.4 mm].
e	Nominal orbit radius [0.180 mm].
e_x, e_y	Orbit amplitudes in the X and Y directions
f_r, f_t	radial and tangential force per unit length acting at axial location Z_j.
h	Local film thickness [m]
L	SFD journal length [31.1 mm].
P	Film dynamic pressure [kPa].
r, t	Radial and tangential coordinates.
X, Y	Horizontal and vertical coordinates and journal center displacements [m].
T	Temperature [°C].
Z_j	Axial location of pressure measurements [mm]. Z_1 (5.6 mm), Z_2 (16.7 mm).
ε	e/C. Dimensionless orbit radius
θ	Circumferential coordinates [rad]
μ	Lubricant viscosity [Pa.s].
ω	Journal whirl frequency [rad/sec].

LIST OF TABLES

LIST OF FIGURES

INTRODUCTION

Squeeze film dampers (*SFDs*) are effective means for force isolation and energy dissipation in high-speed turbomachinery. SFD design, however, remains empirical at best since predictive models derived from Classical Lubrication do not account for the effects of air ingestion; most persistent for operation with low levels of feed pressure and high whirl speeds [1].

Two characteristic squeeze film actions take place in a *SFD* during a period of journal whirl motion. As the film thickness (*h*) decreases (*dh/dt* <0, positive squeeze), the lubricant develops hydrodynamic pressures above ambient and proportional to the journal whirl speed. On the other hand, as the local film increases (*dh/dt* >0, negative squeeze) the dynamic film pressure falls below ambient leading either to lubricant cavitation, or to *air entrainment* if not enough lubricant is available to fill the local gap. Low feed pressures (reduced flow rates), high whirl speeds, and operation with large journal orbital motions (i.e. traversing critical speeds, blade losses or transient vibrations) make imminent the ingestion of air into the damper film lands; thus affecting greatly its ability to generate damping forces [2, 3].

Lubricant *vapor cavitation*, *gaseous cavitation* and *aeration* are the three types of film rupture known in steadily loaded journal bearings [4]. These film rupture forms may also occur in dynamically loaded journal bearings and *SFDs*, albeit showing more complicated flow patterns. In statically loaded journal bearings, as Figure 1a illustrates, the air or vapor cavity occupies a stationary zone, bounded on one side by lubricant (full film) and vented to the gaseous media on the other side (discharge port). However, cyclic (periodic) loading produces ingestion/expulsion of air into/out from the lubricating film [1, 2]. The appearance of large and irregular air fingers migrating throughout the bearing clearance is characteristic of this film rupture form; see Figure 1b. In some instances, gas bubbles remain trapped within the fluid as the film pressure rises above ambient, and strong flow reversals aggravate air ingestion.

Lubricant vapor and gaseous cavitation phenomena differ markedly with the features and ultimate effects of air entrainment. Unfortunately, the technical literature is often misleading and the terms *gaseous cavitation* and *air entrainment* are used indiscriminately to describe the same phenomenon. Mineral lubricants contain dissolved gases with a saturation pressure slightly below ambient pressure. Early, during the negative squeeze action, sub-ambient pressures are developed and non-condensable gas (air) comes out from solution. This phenomenon is properly referred as *gaseous cavitation*. In degassed lubricants, the pressure continues to fall and oil

1

vaporization (*vapor cavitation*) may occur. However, when the film clearance connects to a large gaseous plenum, air is easily drawn into the film lands by the suction generated as the local clearance "stretches".

Cole and Hughes [5] report visual observations of film extent and gaseous cavitation in dynamically loaded journal bearings. By extension, cavitation in *SFD*s has since been considered to be of a similar type. White [6] questions this rationale in lieu of flow visualizations conducted on a test *SFD*, and which revealed finger-like cavities, growing and shrinking during a whirl cycle. Marsh [7], referring to the experimental results in [6], derived test *SFD* forces that are just a fraction, 5 to 25 % in magnitude, of the forces predicted using Classical Lubrication Theory. Bansal and Hibner [8] forward further experimental results that evidence the inadequacy of Reynolds equation to predict damper reaction forces. The authors speculate that the deviation is due to fluid compressibility caused by sub-atmospheric pressures liberating dissolved gases and creating a two-phase fluid. Walton et al. [9] used high-speed photography to reveal flow patterns in a SFD executing circular centered orbits, and again note severe discrepancies with accepted lubrication theory predictions.

Zeidan and Vance [3] identified five regimes of cavitation in a *SFD* according to its operating conditions, and with air entrainment occurring at large amplitudes of journal motion. Flow visualization revealed the formation of a *bubbly mixture*, with air bubbles persisting even in above ambient pressure zones. Radial and tangential forces estimated from the measured dynamic pressures show a nonlinear characteristic akin to that of a softening spring. Diaz and San Andrés [2, 10-12] have conducted the most comprehensive experiments to date, and report the evolution of film pressures during a period of journal motion for increasing contents of air in a controlled lubricant mixture (from pure oil to 100% air). A (synchronous) period-averaging scheme filtered the random fluctuations and spikes in the recorded pressures. The measurements evidence decreasing peak-to-peak pressures (p-p) and *SFD* reaction forces for increasing air contents in the lubricant. The authors recently forwarded a predictive analytical/empirical model that correlates well with their measurements [2].

The present reports continues the research work of San Andrés and Diaz, and forwards measurements of dynamic film pressures and high-speed photographs (video recordings) of the flow field in a *SFD* operating with natural free air entrainment. The experiments were conducted

in an open-ended damper with moderately large journal orbital motions ($\varepsilon_c \rightarrow$ 0.55-0.75) and whirl frequencies ($\omega \rightarrow$ 8.33-50 Hz).

DESCRIPTION OF TEST RIG

The experiments were conducted on a circular-centered orbit SFD operating with one end vented to ambient [10]. Figure 2 depicts a schematic view of the test rig, whose open-end provides a natural path for air entrainment into the squeeze film zone. The damper journal and its ball bearing are mounted on a rigid shaft with an eccentric collar that produces the circular orbits at a whirl frequency synchronous with the shaft rotational speed. The damper journal length (L), diameter (D) and radial clearance (C) are 31.1 mm, 129.4 mm, and 0.254 mm, respectively. The nominal orbit radius (e) is 0.180 mm (e/C=0.71). The uncertainty in the damper dimensions including its clearance and orbit radius is ±0.0127 mm (±0.5 mil).

An ISO VG 68 lubricant was employed in the tests. The oil has a density of 877 kg/m^3 and viscosity of 156.5 cPs at 22.4 $^\circ$C and 56.9 cPs at 40 $^\circ$C, respectively. Table 1 reports measured oil viscosities at increasing temperatures. A DC motor driven gear pump delivers oil to the damper through the inlet holes. A digital flow meter displays the amount of oil fed into the damper. The transparent Plexiglas damper housing contains four strain gauge (absolute) pressure transducers located at two axial planes (one at Z_1 = 5.6 mm and three at Z_2 = 16.7 mm from the sealed end) and three circumferential positions (0°, 150° and 210°), see Figure 3. K-type thermocouples record the lubricant inlet and outlet temperatures. A T-type thermocouple, flush with the inner diameter of the housing, senses the film temperature at the Z_2 plane. Eddy current (non-contacting) displacement transducers measure the journal displacements in two orthogonal planes. The motion signals are used to verify the journal circular motion, establish the orbit centering, and provide a direct estimation of the film thickness.

Journal displacements and film dynamic pressures are acquired with a dedicated DAQ system and stored in a PC. Temperatures, feed and discharge static pressures, flow rate and electrical power are recorded manually from the instrumentation and logged into the DAQ software. A high-speed digital camera with a recording capacity up to 3000 frames/s was used to obtain photographs of the flow patterns.

EXPERIMENTAL PROCEDURE

Measurements of film dynamic pressures, journal motion, film temperature, and inlet and outlet port conditions were performed for gradual increments of the oil flow rate while maintaining a constant rotor speed from 500 to 3,000 rpm, with increments of 500 rpm. The lubricant flow rate was increased discretely (~0.1 l/min) until the return auxiliary pump was not able to evacuate all the lubricant, and the discharge plenum started to flood (typically beyond 0.8 l/min). At the highest flow rate, the main pump was turned-off momentarily and an auxiliary pump evacuated lubricant from the discharge plenum. Then, the main pump was turned-on again, and the video recording triggered once a uniform flow was attained and the squeeze film flow pattern evolved. The movie recording stopped before having a semi-flooded discharge condition.

Table 2 presents a summary of the test conditions and main static measurements; namely rotor speed, lubricant flow rate and feed pressure, film and inlet/ outlet port temperatures, and the motor drive power. The DAQ sampling rate for displacements and dynamic pressures was set to 1000 samples/s with 2048 data points/signal in each experiment. Table 3 reports the number of periods of pressure recorded at each speed and the number of data points/period.

Estimates of the fluctuations on the instantaneous peak-to-peak (p-p) pressure were determined by finding the *lowest ever* and *highest ever* magnitudes over the elapsed testing time. Period averaged orbit amplitudes in the horizontal (X) and vertical (Y) directions, as well as orbit offsets, followed a similar procedure from estimation of the maximum and minimum journal displacements in each direction.

The *SFD* is circumferential symmetric, and thus, the dynamic pressure field "rotates" at the same speed as the journal whirl frequency. Diaz and San Andrés [10-12] detail the time dependency of the measured variables and the temporal fluctuations associated with bubbly lubricant mixtures. Presently, dynamic pressure profiles recorded during 14 full periods of journal motion are period averaged to render smooth fields characteristic of a full cycle of journal motion. Note that he instrumentation uncertainty is much smaller that the uncertainty arising from the dynamic variation in the recorded film pressure and journal displacements.

Digital films were recorded at 500 frames/s in all experiments. White tissue paper wrapped around the apparatus provided a suitable lighted environment and reduced the sharp reflection of the intense light on the damper surface. The camera lens was adjusted to span a window 30° wide in the circumferential direction and the whole damper axial length. The lubricant was colored

with an inert dark-blue powder dye to enhance the contrast between the lubricant and the ingested air fingers. The photographs properly synchronized with the journal displacements and the dynamic pressure measurements evidence characteristic flow patterns very close to actual practice. Table 4 lists the specifications of the recorded films. Composite digital video clips of flow fields, measured dynamic pressures and journal motion for selected operating conditions are available upon request (see http://metrib.tamu.edu/rotorlab.htm).

EXPERIMENTAL RESULTS

Figure 4 depicts the gauge feed pressure to vary linearly with the lubricant inlet flow rate for each operating speed. Within the speed range (500-3,000 rpm), whilst a constant flow rate was maintained, a small increment in the pressure supply (21 kPa, at most) ensued between the lowest and highest journal speeds tested. Do note that the lubricant temperature did not remain constant during the experiments as detailed below.

Table 2 lists the measured static parameters for each test conducted as the shaft speed increased. The tables show the lubricant inlet flow rate and feed pressure, the inlet and outlet lubricant temperatures, the SFD journal (dimensionless) orbit radius, and the power delivered by the drive motor. In each test, the shaft speed was maintained as the lubricant supply pressure increased to span feed conditions from nearly no flow (starvation) to full through flow rates at high feed pressures. Note that significant variations of the lubricant temperature at the inlet port were recorded during the numerous tests; see Figure 6 later. Thus, the measurements evidence an inlet lubricant viscosity determined by the testing time. Warm lubricant coming out from the damper mixed with the oil in the sump and raised its temperature. Note that each experiment took about 20-25 minutes for completion, including setting up the DAQ system.

Figure 5 shows measured lubricant viscosities for a wide range of temperatures at atmospheric pressure. Figure 6 depicts the film temperatures recorded at location Z_2 versus the operating speed for each feed pressure level. Observe that the film temperature is not speed dependent but rather testing time dependent, i.e. it increases due to the time elapsed while conducting the experiments.

In most experiments the lubricant temperature at the inlet and outlet ports shows a difference of only 2 °C, while the film temperature at Z_2 could be 10 °C higher than the inlet temperature. The results thus evidence very low lubricant heat convection rates since the flow rates were

rather small at the onset of each set of experiments. Thus, as a set of measurements started, the journal and damper warmed up rapidly, and the film temperature recorded corresponds to that of the housing and not the actual one within the fluid film. Once the higher flows were achieved the damper as well as the journal were very hot and the lubricating flowing through the *SFD* was unable to remove the dissipated heat during the remaining test time.

Journal Orbit Amplitudes and Offset

Figure 7 shows the journal orbit amplitudes in the X and Y-directions as the feed pressure increases for tests at 500, 1,500 and 3,000 rpm. Results are shown in dimensionless form with the nominal clearance (C) as the reference value. The orbital amplitudes differ slightly in both directions, and most notably decrease sharply as the feed pressure increases to ~100 kPa. It is worth noting that the supply pressure causes an axial force pushing the journal against the O-ring face of the test *SFD*. This mechanical (dry-friction like) load forces smaller orbits while increasing the power to drive the test rig. At low speeds the orbit amplitudes are stable and repetitive. Estimated first order uncertainties (variability) in the orbit amplitudes are on the order of $\pm 1\%$. As the speed increases the orbit amplitudes fluctuated in an intermittent manner. Variations in the orbit amplitudes are up to $\pm 5\%$ in the X-direction and $\pm 3\%$ in the Y-direction at 1500 rpm, and up to $\pm 3\%$ in both directions at 3,000 rpm.

Figure 8 displays the amplitudes of orbital motion (X, Y) versus the operating speed for three feed pressure levels (40, 110 and 150 kPa). Vibrations of the drive motor belt cause the visible crest at 2,000 rpm. Figure 9 shows that the damper journal remained nearly centered within 10% of its clearance. From 500 to 1,500 rpm the orbit offset in the X-direction increases, while that in the Y-direction remains fairly constant. From 1,500 to 3,000 rpm the opposite effect occurs. The transition is probably related to the effect of the transmission belt vibrations. Figure 10 depicts dimensionless journal orbits at 500 and 3,000 rpm for no oil feed (dry damper) and two feed pressures. The journal orbits become more elliptic as the feed pressure and rotor speed increases.

Film Dynamic Pressures and Flow Visualization

Air naturally entrained into the damper clearance for flow conditions not flooding the damper discharge plenum. Figure 11 shows measured film pressures at $(210°, Z_2)$ and journal X-motion at 1,500 rpm (25 Hz) and feed pressure equal to 55 kPa (8 psig). The pressure signals have been

6

shifted by known phase angles relative to the journal displacement signal. Note the fluctuating and intermittent behavior of the dynamic pressure with sudden pressure spikes and variations of the peak-to-peak (p-p) pressure between consecutive periods of journal motion. Furthermore, a nearly uniform pressure zone evolves around the location of maximum film thickness with sub-ambient pressures occurring on each half-period of (negative) squeeze motion. Despite the random irregularities there is an apparent periodicity as revealed by the (synchronous speed) period averaged pressure[1] also displayed in the Figure.

Figure 12 shows characteristic (period averaged) dynamic pressure profiles at $(150°, Z_2)$, $(210°, Z_2)$ and $(180°, Z_2)$ and the X-journal motion for a test at 1,500 rpm and 55 kPa (8 psig) feed pressure. The dynamic pressures at $150°$ and $210°$ are shifted by phase angles with respect to the displacement signal. The procedure allows direct correlation of the generated dynamic pressures and the instantaneous journal displacement. In the discussion, the dynamic film pressure at the camera location $(180°, Z_2)$ is considered as the simple average of the pressures recorded at $150°$ and $210°$. Note the similarity of the (synchronous speed) period-averaged pressure profiles obtained at the different angular locations. The experimental results thus evidence that the multiple period-averaged film pressure does rotate around the journal in synchronicity with the shaft speed.

Numbered circles in Figure 12 correspond to photographs of the flow field at key instances within three periods of journal motion and displayed in Figure 13. The period of motion is 0.040 s at 1,500 rpm (25 Hz). The photographs in the same row correspond to a single period of journal motion, namely 1-6 (1st period), 7-12 (2nd period) and 13-18 (3rd period). The picture frames in the same column refer to the flow pattern observed at about the same instant of time relative to a journal period of motion. From left to right, the journal goes through the minimum film thickness at positions 2, 8 and 14; then the film thickness increases ($dh/dt>0$, negative squeeze) to frames (5, 11, 17), and the local film decreases ($dh/dt<0$, positive squeeze) in frames (6-7), (12-13) and (18). Peak dynamic pressures occur at frames (1), (7) and (13) just before the local minimum film thickness.

---

[1] Diaz and San Andrés [16, 17] earlier experiments demonstrated the striking similarity between the pressure profiles resulting from air entrainment and those obtained with a *homogeneous* (controlled) bubbly mixture. These authors introduced a (synchronous speed) period ensemble-averaging to filter the pressure spikes and random variations while keeping the most relevant features representative of many periods of journal motion.

In general, the photographs evidence air ingestion as large irregular finger-like cavities moving from the open plenum towards the *SFD* sealed end, in particular at those instances where the film rate of change (*dh/dt*) is maximum as depicted in frames (4-5), (10-11) and (16-17). The large air striations (at nearly ambient pressure) migrate rapidly into the film lands. The large zones of air entrainment persist even at the beginning of the positive squeeze zone, i.e. while the local film decreases (*dh/dt*<0), as seen in frames (6), 12) and (18). However, most of the air is expelled within a fraction of the journal periodical motion while the film pressure builds up rapidly above ambient, as frames (1), (7) and (13) depict. The drop from peak film pressure to the sub ambient value is also rapid; and frames (2), (8) and (14) show the beginning of air ingestion and, in some instances, pressures near (or just below) zero absolute.

A complete analysis of the flow patterns recorded for several journal periods of motion evidence that no more than two consecutive periods of motion show similar flow patterns at each relative instant of motion. For example, frames 13 and 14 in Figure 13 show zones of entrapped air cavities able to withstand the maximum pressure, and remaining even as the film thickness reaches a minimum about 210 kPa and 130 μm, respectively (also refer to circles 13 and 14 in Figure 12). Thus, the amount of air entrained differs on each period of motion, and its persistence in the high-pressure region leads to pressure spikes as the local film thickness decreases. The large striations and fingers ingested into the damper lands obviously contain air drawn from the vented end of the test damper. The contents of the minute rounded-like cavities could be mostly vapor lubricant rather than dissolved gases, in lieu of the low dynamic pressures recorded.

Figure 14 shows a series of photographs displaying the inception and persistence of local lubricant cavitation while the pressure drops from peak to sub ambient values. The time instants and pressures (see captions) correspond to the pressure profile shown in Figure 12. Frame (a) shows some cavities that have persisted in the high-pressure zone. Next in frame (b), a flow reversal occurs at the instant of minimum film thickness and local pressure just below ambient [circle # 2, Figure 12]. As the film thickness begins to increase (*dh/dt* >0), frames (c) and (d) show the growth of the cavity volumes and the emergence of others into the visual field. The small size cavities may contain lubricant vapor since the local film pressure is close to zero

absolute, although the time span for the phase change process is too short[2]. Frame (e) at the instant of lowest recorded pressure (just below zero absolute) displays enlarged cavities, resulting from the merging (coalescence) with others. Note that there is still a large portion of the film covered with lubricant, and able to sustain some tension.

Frame (f) in Figure 14 depicts a digitally enhanced version of frame (e) (also frame 3 in Figure 13). The gas cavity enclosed within a circle shows some small "inclusions". The digital image processing displays their edges, thus revealing its liquid content, otherwise they would diffuse within the enclosing cavities. The liquid drops could be attached to the bearing or journal surfaces, or suspended within the larger irregular gas (air) cavity. The presence of these liquid drops, as remnants of the full film of lubricant, may be related to the surface finish of the damper housing and journal.

Figure 15 depicts other measurements of journal motion and film pressure versus time, and flow pictures for two feed pressures and rotor speed conditions: (a) 110 kPa (16 psig) and 500 rpm, and (b) 151 kPa (22 psig) and 1,000 rpm. In (a), note that a larger feed pressure helps to reduce the extent of air ingestion (compare with frames 5, 11 and 17 in Figure 13). In (b), even a larger feed pressure cannot prevent the onset of lubricant vaporization for operation at higher rotor speeds (compare with frames 2, 8 and 14 in Figure 13). The flat portion in the pressure profiles recorded at Z_1 is at near zero absolute pointing out to a zone of lubricant vaporization.

Figure 16 displays the multiple-period (synchronous speed) averaged film pressures for increasing journal speeds at the different locations of measurement and for a range of feed pressures. The graphs on the left and right columns correspond to axial locations Z_1 and Z_2, respectively. The test results at the lowest speeds (500 and 1,000 rpm) show a marked difference in the pressure profiles for low and high feed pressures. At low feed pressures, the pressure field shows a typical zone of uniform pressure at ambient conditions and relatively small time regions where the pressure rapidly changes, either towards a peak positive value or sub ambient towards zero absolute. In these measurements, air ingestion is most prevailing. On the other hand, increases in the feed pressure (larger flow rates) reduce air ingestion and the pressure field evolves continuously from low to high to low pressures, in some instances developing vapor lubricant cavitation, particularly at axial location Z_1. The measurements at the highest speed

---

[2] Most likely the cavities contain air that comes out of solution as the film thickness locally increases. Their volume grows and becomes visible then. Note that the abrupt pressure reduction from ambient to a sub zero value occurs in only 0.006 seconds, a time too short to ensure a phase change (typically a slow process).

(3,000 rpm) show dynamic pressures typical of air ingestion in spite of the increases in feed pressure (larger through flow rates).

Figure 17 evidences large air fingering even for a relatively high-feed pressure (193 kPa). The measured pressure profiles closely resemble those obtained earlier with a controlled bubbly mixture [16]. Thus, large lubricant flow rates (high feed pressure) and low operating speeds delay air entrainment in *SFD* operation. High inlet pressures are desirable although the cost and size of such an arrangement is not affordable in practical applications.

It is important to note that the repeatability of the measurements increased as the lubricant feed pressure increases. At low feed pressures the fluctuations in the measured dynamic pressures and journal displacements are significant due to the random distribution of the ingested air fingers within the damper lands.

Peak dynamic pressures and estimated film forces

Figure 18 shows the recorded peak-peak (p-p) dynamic film pressures versus feed pressures for speeds of 500, 1,500 and 3,000 rpm. Figure 19 displays similar results as a function of the rotor speed and ranges of feed pressures. The overall temporal variation (first order uncertainty) in the p-p pressures from (no less than) 16 periods of motion at the Z_1 and Z_2 planes are $\pm 4\%$ at 500 rpm, $\pm 12\%$ at 1,500 rpm and $\pm 23\%$ at 3,000 rpm, respectively. The analysis of the recorded test data then shows that as the operating speed increases, the fluctuations in the p-p dynamic pressures increase since air entrainment becomes more severe. The p-p pressures recorded at the Z_1 plane (Figure 19a) remain fairly constant with respect to variations in the feed pressure and speed. However, the p-p pressures recorded at the Z_2 plane (Figure 19b) show a somewhat irregular behavior as the speed increases. Most importantly, do note that the p-p pressures remain relatively constant for increasing feed pressures and rotor speeds. This apparently contradictory behavior is probably related to the drop in lubricant viscosity (higher temperature) as the testing progressed.

The squeeze film forces $(f_r, f_t)_{(Z)}$ per unit length in the radial and tangential directions are estimated from numerical integration of the measured dynamic pressures over a period of journal motion, i.e.

$$f_{(Z)} = (f_r + i \cdot f_t)_{(Z)} = \frac{-\omega \frac{D}{2}}{n} \cdot \int_{t_o}^{t_o + n \cdot T} P_{(t,Z)} \cdot e^{-i \cdot \left[\omega \cdot (t - t_o) + \theta\right]} \, dt \qquad (1)$$

The procedure also gives the ensemble radial and tangential forces (f_r, f_t) by averaging the forces obtained from the pressures at the different angular locations in the same axial plane.

Figure 20 depicts the film forces versus the feed pressure at three operating speeds and at the axial locations of measurement. The experiments at 500 rpm reveal an increase in tangential (damping) forces ($f_{t(Z_2)}$) towards an asymptotic value, and decreasing radial forces ($f_{r(Z_2)}$) as the feed pressure raises. At 1,500 rpm, the tangential force grows for the range of the feed pressures, while the radial force remains relatively constant. The same rationale follows at 3,000 rpm, although the radial force at plane Z_1 appears to grow slightly. Thus raising the feed pressure causes flooding of the squeeze film region and diminishes the effects of air entrainment (lubricant cavitation as well). Note that the average forces derived from pressures recorded at three angular locations of measurement (Z_2) do not differ much from the individual forces at each circumferential location. Thus, the measurements indicate the period-average pressure field is representative of the dynamic behavior at all circumferential locations.

Most importantly, however, the forces derived from the experimental film pressures decrease rapidly as the journal speed (whirl frequency) increases. Figure 21 shows the film forces, radial and tangential, versus journal speed for the range of feed pressures in the tests (at Z_2 plane). Note that the radial forces are relatively smaller than the tangential damping forces at low speeds. However, the damping (tangential) forces drop rapidly as the whirl frequency increases. This finding opposes dramatically analytical predictions based on Classical Lubrication Theory and evidences the paramount effect of air entrainment on degrading SFD dynamic forced performance. Refer to the discussion on the pressure fields and photographs of air entrainment to realize that air ingestion and entrapment becomes more prevalent as the whirl frequency raises, and increasing the feed pressure aids little to ameliorate the loss in dynamic forced performance.

The conclusions derived, however, must be taken with caution since, in the experiments, the lubricant heated rapidly as the whirl speed increased. Thus, the lubricant effective viscosity also decreased rapidly. This flaw in the experimental measurements will be corrected in the near future by conducting more measurements with a controlled (uniform) lubricant temperature.

CLOSURE

Experiments were conducted on a controlled orbit test *SFD* operating with an end plenum vented to ambient conditions. Measurements of the dynamic film pressures at two axial planes and journal motion were performed for increasing journal speeds to 3,000 rpm and a range of feed pressures to 250 kPa (37 psig). High-sped video recordings at selected operating conditions revealed the unique features of the flow field within the *SFD*. Digital movie clips showing the flow field and pressure and motion measurements are available for further analysis.

The experiments show that air entrainment leading to the formation of irregular gas fingering and striation patterns is a natural phenomenon in *SFD*s operating with low levels of external pressurization (low lubricant through flow rates). Operation at high whirl frequencies always shows this persistent phenomenon even for large feed pressures. *SFD* film damping (tangential) forces decrease as the journal whirl speed raises, in opposition to predictions based on Classical Lubrication Theory.

The results of the extensive experiments are not conclusive since, unfortunately, the lubricant temperature did not remain uniform over the long test time that spanned the range from low to high feed pressures. Thus, the experimentally derived film forces include the (yet not quantifiable) effect of a decreasing viscosity as the feed pressure increases. Controlled temperature experiments will be performed this Summer to confirm or disprove the test results hereby presented.

ACKNOWLEDGEMENTS

REFERENCES

[1] San Andrés, 2000, "Squeeze Film Dampers – Design and Operating Issues," *Class Notes on Modern Lubrication*, Texas A&M University.

[2] Diaz, S. and L. San Andrés, L., A Model for Squeeze Film Dampers Operating with Air Entrainment and Validation with Experiments," accepted for publication at ASME Journal of Tribology, May 2000 (ASME Paper 2000-Trib-207).

[3] Zeidan, F. Y., and Vance, J. M., 1990, "Cavitation Regimes in Squeeze Film Dampers and Their Effect on the Pressure Distribution," *STLE* Tribology Transactions, Vol. 33, pp.447-453.

[4] Dowson, D. and Taylor, M. 1974, "Fundamental Aspects of Cavitation in Bearings," *Proceedings of the 1ˢᵗ Leeds-Lyon Symposium on Tribology, University of Leeds*, England, pp. 15-28.

[5] Cole, J. A. and Hughes, C. J., 1957, "Visual Study of Film Extent in Dynamically Loaded Complete Journal Bearings," Proc. Lub. Wear Conf., pp. 147-149.

[6] White, D. C., 1970, "Squeeze Film Journal Bearings," Ph. D. Dissertation, Cambridge University.

[7] Marsh, H., 1974, "Cavitation in Dynamically Loaded Journal Bearings," *Proceedings of the 1ˢᵗ Leeds-Lyon Symposium on Tribology, University of Leeds*, England, pp. 91-95.

[8] Bansal, P. N and Hibner, D. H, 1978, "Experimental and Analytical Investigation of Squeeze Film Bearing Damper Forces Induced by Offset Circular Whirl Orbits," *ASME* Journal of Mechanical Design, Vol. 100, pp. 549-557, July.

[9] Walton, J., Walowit, E., Zorzi, E., and Schrand, J., 1987, "Experimental Observation of Cavitating Squeeze Film Dampers," *ASME* Journal of Tribology, 109, pp. 290-295.

[10] Diaz, S. E., and San Andrés, L. A., 1997, "Measurements of Pressure in a Squeeze Film Damper with an Air/Oil Bubbly Mixture," *STLE* Tribology Transactions, Vol. 41, 2, pp. 282-288.

[11] Diaz, S. E., and San Andrés, L.A., 1998, "Reduction of the Dynamic Load Capacity in a Squeeze Film Damper Operating with a Bubbly Mixture", ASME Journal of Engineering for Gas Turbines and Power, Vol. 121, pp. 703-709.

[12] Diaz, S., and L. San Andrés, 1999, "Air Entrainment vs. Lubricant Vaporization in Squeeze Film Dampers," *ASME* Paper 99-GT-187.

Table 1. Viscosity of ISO VG 68 lubricant: measurements

Specific gravity = 0.877

Temperature ° C	Viscosity (cPs)
22.4	156.5
24.6	139.4
26.4	125.6
28.2	109.2
30.1	98.2
33.3	79.1
36	70.2
40	56.9

$\mu = \mu_{ref}\, e^{\alpha(T-T_{ref})}$, where μ_{ref} = 156.5 cPs, T_{ref} = 22.4° C, and α = -0.057/°C.

Table 2. Test conditions: speed, oil inlet flow rate, feed pressure, temperatures, orbit radius (ε_c), and drive power.

500 rpm

Oil Inlet Flow (Q)	ΔQ	Gauge Feed Pressure (P)		ΔP		Temperatures Inlet	Temperatures Plane Z₂	Temperatures Outlet	ε_c	Drive Power
lt/min	lt/min	psi	kPa	psi	kPa	°C	°C	°C		Watts
0.073	0	5	34.45	0	0	22.2	24.4	23.9	0.71	230.3
0.215	0.142	12	82.68	7	48.23	22.2	31.7	25.0	0.64	255
0.311	0.096	16	110.24	4	27.56	23.3	33.9	25.6	0.64	260
0.421	0.110	18	124.02	2	13.78	26.1	36.7	27.2	0.64	254.8
0.516	0.095	22	151.58	4	27.56	26.7	36.7	28.9	0.64	244.8
0.625	0.109	26	179.14	4	27.56	26.7	36.7	28.3	0.64	249.6

1000 rpm

Oil Inlet Flow (F)	ΔF	Gauge Feed Pressure (P)		ΔP		Temperatures Inlet	Temperatures Plane Z₂	Temperatures Outlet	ε_c	Drive Power
lt/min	lt/min	psi	kPa	psi	kPa	°C	°C	°C		Watts
0.0728	0	5	34.45	0	0	22.2	25.6	23.9	0.66	254.4
0.128	0.055	8	55.12	3	20.67	22.2	27.8	23.9	0.62	400.2
0.192	0.064	12	82.68	4	27.56	22.8	31.1	25.0	0.59	387.6
0.322	0.130	16	110.24	4	27.56	23.9	33.3	25.6	0.59	401.2
0.415	0.093	19	130.91	3	20.67	25.3	35.8	27.2	0.59	389.3
0.508	0.186	22	151.58	6	41.34	26.1	36.1	27.2	0.59	381.9
0.597	0.089	26	179.14	4	27.56	26.7	36.1	28.3	0.59	381.9
0.706	0.109	27.5	189.48	1.5	10.34	27.2	36.7	28.9	0.59	376.2
0.798	0.092	30	206.70	2.5	17.23	27.8	37.2	29.4	0.59	388.6
1.079	0.281	37	254.93	7	48.23	28.9	36.1	29.4	0.59	376.2

1500 rpm

Oil Inlet Flow (F)	ΔF	Gauge Feed Pressure (P)		ΔP		Temperatures Inlet	Temperatures Plane Z₂	Temperatures Outlet	ε_c	Drive Power
lt/min	lt/min	psi	kPa	psi	kPa	°C	°C	°C		Watts
0.079	0	5	34.45	0	0	22.2	26.1	23.9	0.69	376.2
0.113	0.034	8	55.12	3	20.67	22.2	28.9	23.9	0.65	425
0.211	0.098	12	82.68	4	27.56	22.8	31.1	25.6	0.64	525.1
0.292	0.081	16	110.24	4	27.56	23.9	33.3	26.1	0.61	519.2
0.394	0.102	19	130.91	3	20.67	24.4	36.7	27.2	0.60	525.1
0.493	0.099	23	158.47	4	27.56	26.1	36.5	27.8	0.59	525.1
0.592	0.198	26	179.14	7	48.23	27.2	36.1	28.3	0.59	519.2
0.791	0.199	31	213.59	5	34.45	27.8	37.2	29.4	0.58	519.2

Table 2. (Continued) Test conditions.

2000 rpm

Oil Inlet Flow (F)	ΔF	Gauge Feed Pressure (P)		ΔP		Temperatures			ε_c	Drive Power
lt/min	lt/min	psi	kPa	psi	kPa	Inlet °C	Plane Z_2 °C	Outlet °C		Watts
0.0805	0	5	34.45	0	0	22.2	28.3	23.9	0.75	448
0.207	0.127	12	82.68	7	48.23	22.8	31.7	25.6	0.72	470.4
0.289	0.082	16	110.24	4	27.56	23.9	33.9	26.1	0.68	485.9
0.408	0.119	19	130.91	3	20.67	25.6	37.8	27.2	0.65	497.2
0.488	0.080	23	158.47	4	27.56	26.1	35.6	28.3	0.63	580
0.6	0.112	26	179.14	3	20.67	27.2	36.7	28.3	0.63	580
0.708	0.108	29	199.81	3	20.67	27.8	36.7	29.4	0.61	580

2500 rpm

Oil Inlet Flow (F)	ΔF	Gauge Feed Pressure (P)		ΔP		Temperatures			ε_c	Drive Power
lt/min	lt/min	psi	kPa	psi	kPa	Inlet °C	Plane Z_2 °C	Outlet °C		Watts
0.108	0	6	41.34	0	0	22.2	31.1	24.4	0.71	1055.6
0.205	0.097	12	82.68	6	41.34	22.8	32.2	25.6	0.67	866.4
0.306	0.101	16	110.24	4	27.56	23.9	33.9	26.7	0.64	725.2
0.403	0.097	20	137.80	4	27.56	25.6	36.9	26.7	0.63	725.2
0.506	0.103	23	158.47	7	48.23	26.1	35.6	27.8	0.62	735
0.597	0.091	26	179.14	3	20.67	27.2	36.7	28.9	0.60	823.2
0.703	0.106	28	192.92	2	13.78	27.8	37.2	29.4	0.59	797.5
0.806	0.103	32	220.48	4	27.56	28.3	37.8	30.0	0.57	797.5
0.895	0.089	34	234.26	2	13.78	28.3	37.2	30.0	0.56	792

3000 rpm

Oil Inlet Flow (F)	ΔF	Gauge Feed Pressure (P)		ΔP		Temperatures			ε_c	Drive Power
Lt/min	lt/min	psi	kPa	psi	kPa	Inlet °C	Plane Z_2 °C	Outlet °C		Watts
0.0813	0	6	41.34	0	0	22.2	31.7	24.4	0.70	867
0.207	0.126	12	82.68	6	41.34	22.8	33.3	26.1	0.68	818.3
0.304	0.097	16	110.24	4	27.56	23.9	34.4	26.7	0.66	813.4
0.4	0.096	20	137.8	4	27.56	25.6	36.1	26.1	0.63	813.4
0.503	0.103	22	151.58	2	13.78	26.7	36.7	28.3	0.63	830
0.599	0.096	25	172.25	3	20.67	27.8	37.2	29.4	0.63	885.3
0.695	0.192	28	192.92	6	41.34	27.8	37.8	30.0	0.64	935.2
0.799	0.104	31	213.59	3	20.67	28.3	38.3	30.0	0.63	951.9
0.907	0.108	33	227.37	2	13.78	28.3	38.3	30.6	0.60	1047.8

Characteristic orbit radius $\varepsilon_c = (\varepsilon_x + \varepsilon_y)/2$ (Dimensionless)

Table 3. Settings for data acquisition.

Speed Tested rpm	Number of Data Points/period	Number of Recorded Periods
500	120	17.06
1000	60	34.13
1500	40	51.20
2000	30	68.26
2500	24	85.33
3000	20	102.4

DAQ sampling rate: 1000 points/s
Recorded points per channel: 2048
Recorded time per channel: 2.048 s

Table 4. Descriptive features of recorded films.

General video Format: AVI uncompressed, 512 x 512, 8 Bits, 500 frames/sec
Elapsed time between each frame caption: 0.002 s
Recording time [s] = number of frames / 500 [frames/s]
Recorded # whirl periods = Recorded time [s] * whirl frequency [Hz]

Whirl Frequency Hz (rpm)	Oil Flow Rate lt/min	Feed Pressure KPa (psi)	Movie Clip *.AVI		No. of Recorded Frames	Recorded Time [s]	Recorded Whirl periods	Frames per period	Period of journal motion [s]
8.33 (500)	0.1	55.12 (8)	VR1-400		400	0.8	6.66	60	0.12
8.33 (500)	0.3	110.24 (16)	VR4-180		180	0.36	3.00	60	0.12
8.33 (500)	0.5	151.58 (22)	VR7-86		86	0.172	1.46	60.14	0.12
16.66 (1000)	0.1	55.12 (8)	VR2-400		400	0.8	13.33	30	0.06
16.66 (1000)	0.3	110.24 (16)	VR5-258	*	258	0.516	8.60	30	0.06
16.66 (1000)	0.5	151.58 (22)	VR8-86		86	0.172	2.86	30.07	0.06
16.66 (1000)	0.7	189.48 (27.5)	VR11-86	*	86	0.172	2.86	30.07	0.06
25.00 (1500)	0.1	55.12 (8)	VR3-400	*	400	0.8	20.00	20	0.04
25.00 (1500)	0.3	110.24 (16)	VR6-258	*	258	0.516	12.90	20	0.04
25.00 (1500)	0.5	158.47 (23)	VR9-182	*	182	0.364	9.10	20	0.04
25.00 (1500)	0.7	193 (28)	VR12-86	*	86	0.172	4.30	18.7	0.04

Digital video clips including the flow field, dynamic pressures and film thickness are available for films marked (*) at the URL site http://metrib.tamu.edu/SFDmovies.

The free software Shockwave™ (Flash) player is needed to display the movies on a PC computer.
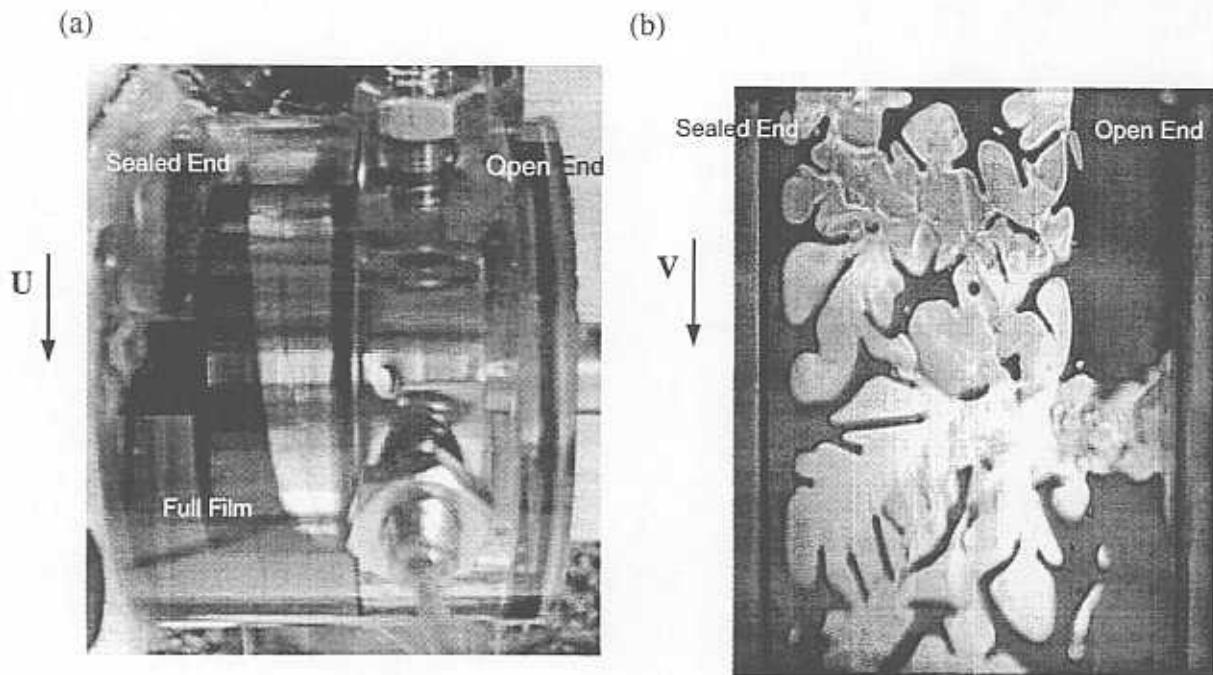
Figure 1. (a) Stationary aerated cavity in a journal bearing. b) Squeeze film flow of an open-ended SFD subject to air entrainment (window span of 30°). U and V denote the journal rotational and whirling speeds, respectively.
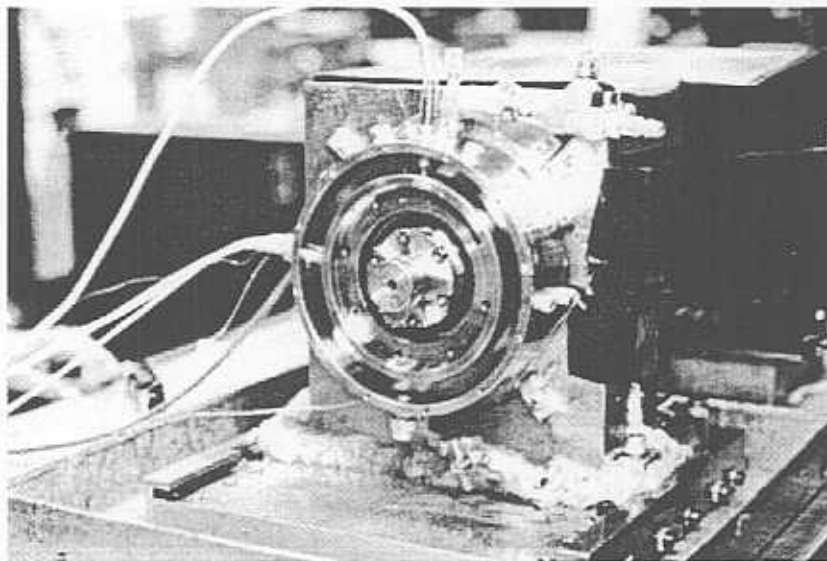
Figure 2. Photograph of test SFD.

17
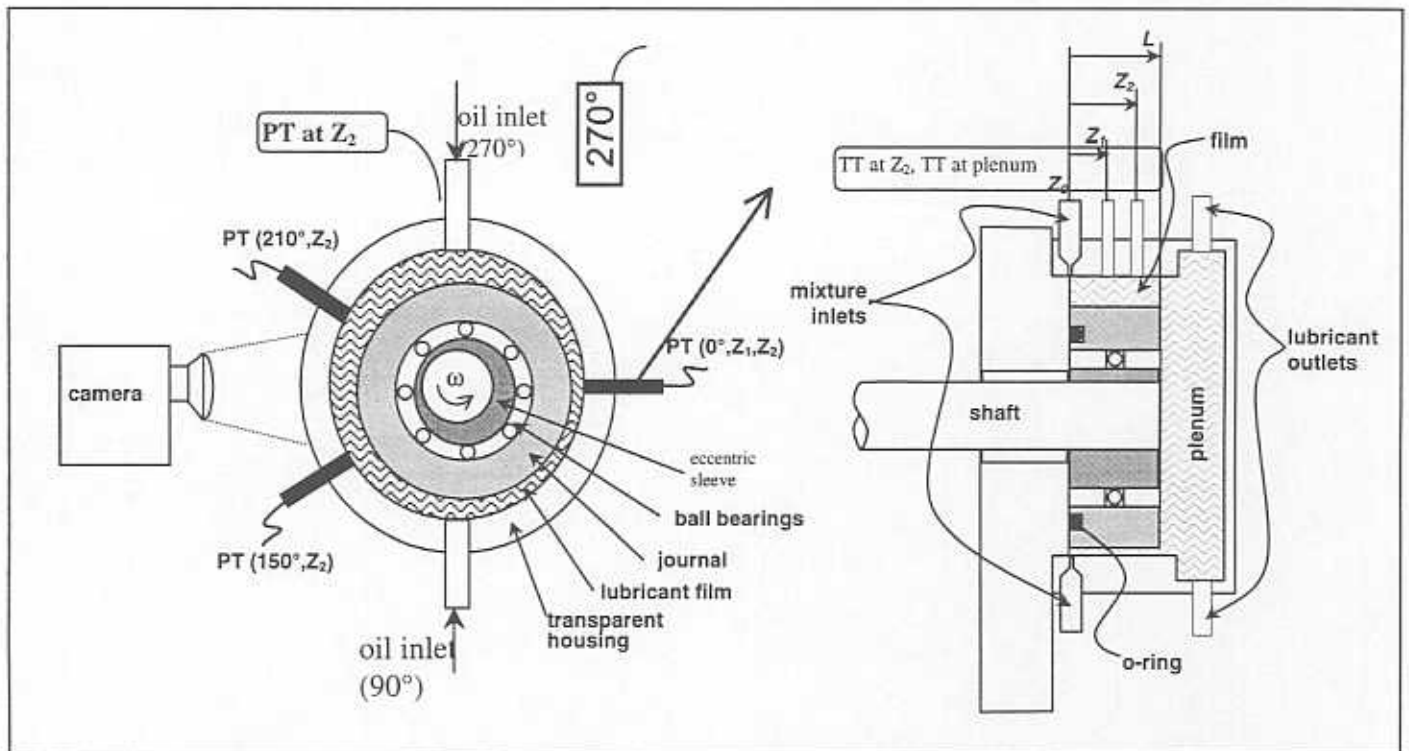
Figure 3. Schematic view of test rig and instrumentation.
L= 31.1 mm (1.22 in), D=129.3 mm (5.10 in), C=0.254 mm (0.010 in),
Z_1= 5.6 mm (0.22 in), Z_2= 16.7 mm (0.66 in), Z_3= 37.1 mm (1.46 in),
PP: Displacement sensor, PT: pressure transducer, TT: Thermocouple, PG: pressure gauge.
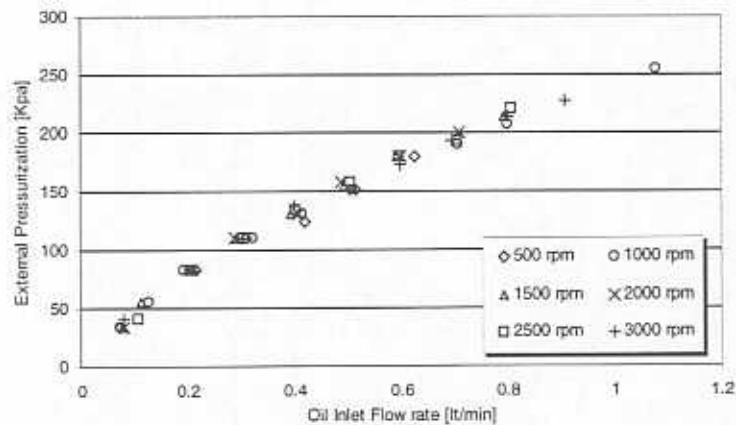
Figure 4. Feed supply pressure (gauge) versus oil inlet flow rate at each test speed.
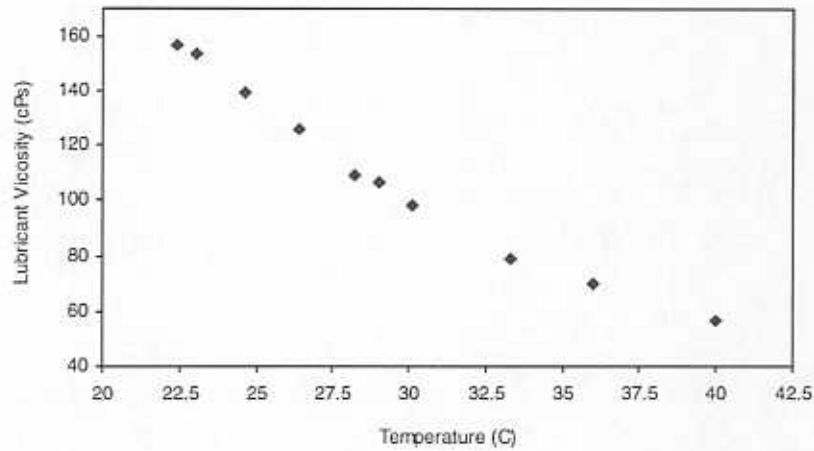
Figure 5. Lubricant viscosity (ISO VG 68) versus temperature: measurements.
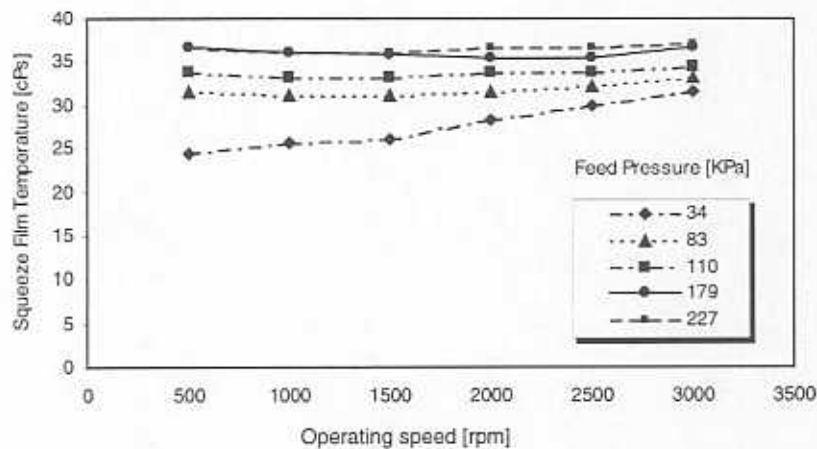
Figure 6. Test film temperature at Z_2 versus operating speed and increasing feed (gauge) pressures.
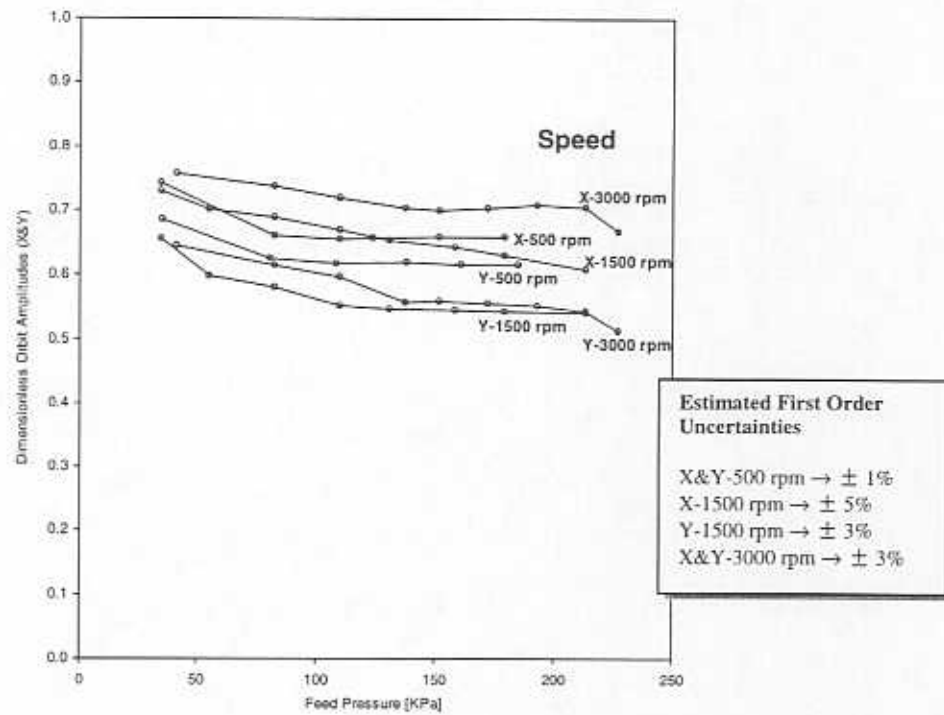
Figure 7. Dimensionless journal orbit amplitudes (X, Y) versus feed pressure for increasing speeds.
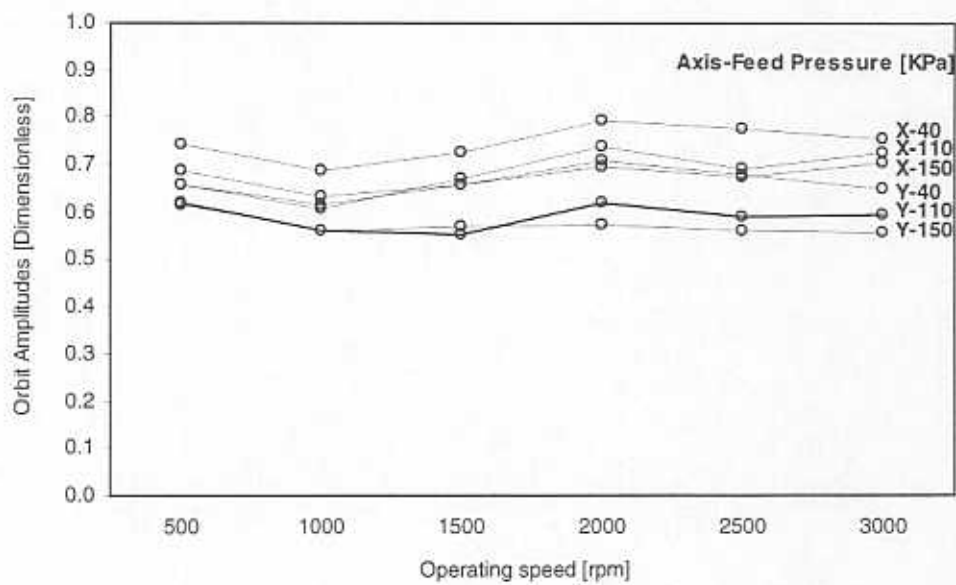
Figure 8. Dimensionless journal orbit amplitudes (X, Y) versus operating speed for increasing feed pressures.
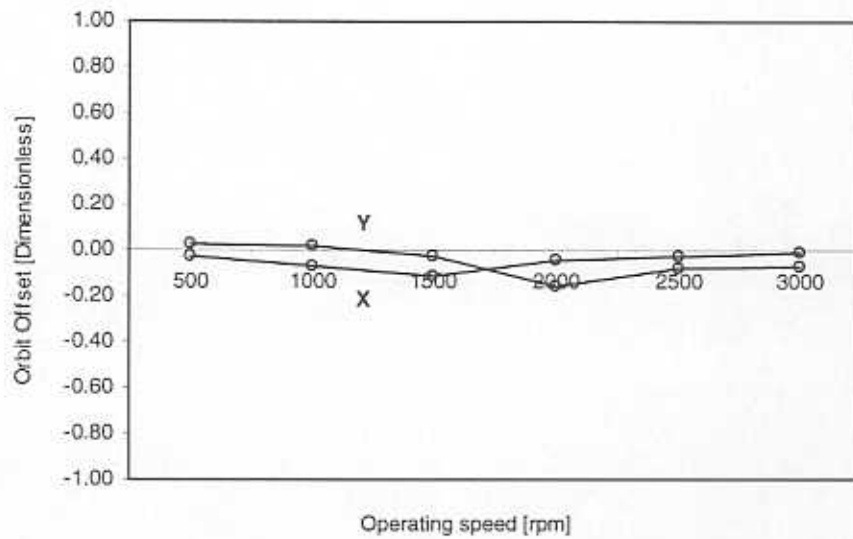
Figure 9. Dimensionless offset for journal orbit versus operating speed.

o: Orbit center of reference (No lubricant feeding).
+: Orbit center at a feed pressure of 82 kPa.
x: Orbit center at a feed pressure of 180 (left)
   and 150 kPa (right).

(a)   (b)
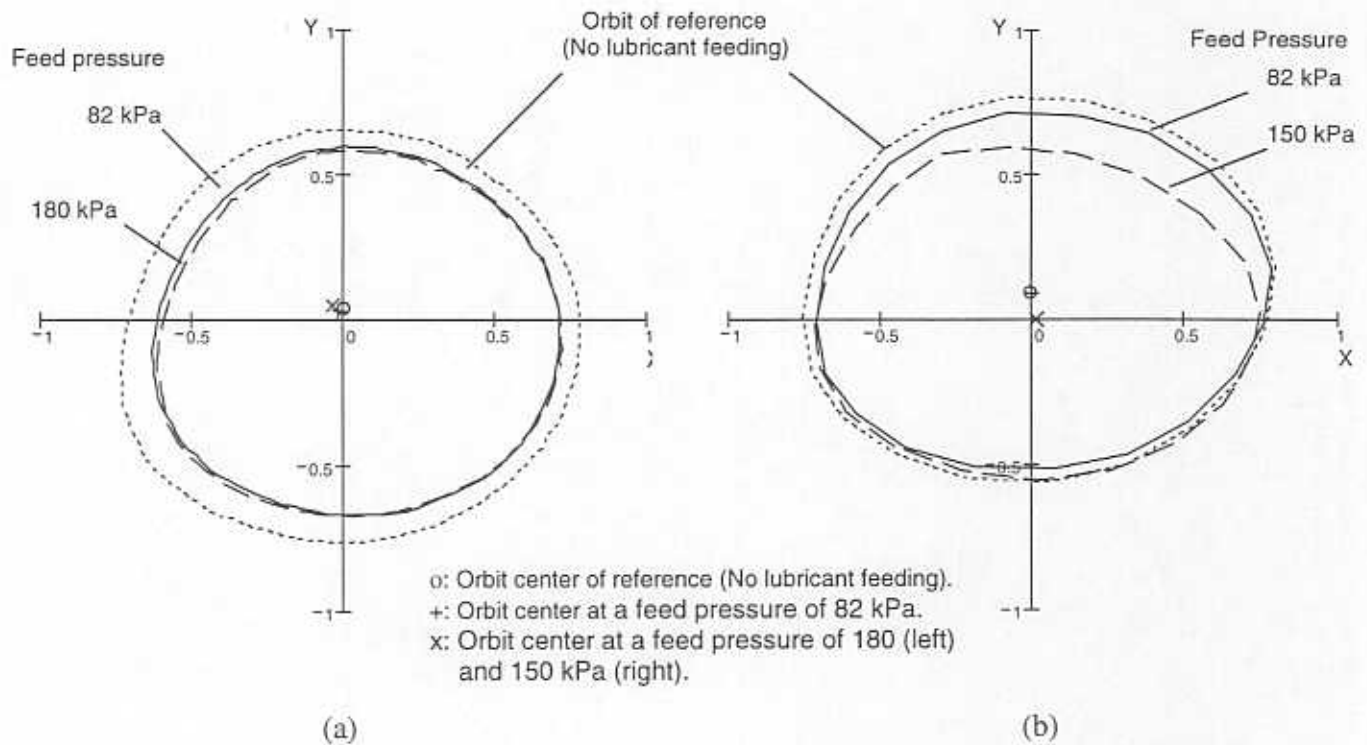
Figure 10. Recorded journal orbits and orbit center at (a) 500 rpm and (b) 3,000 rpm.
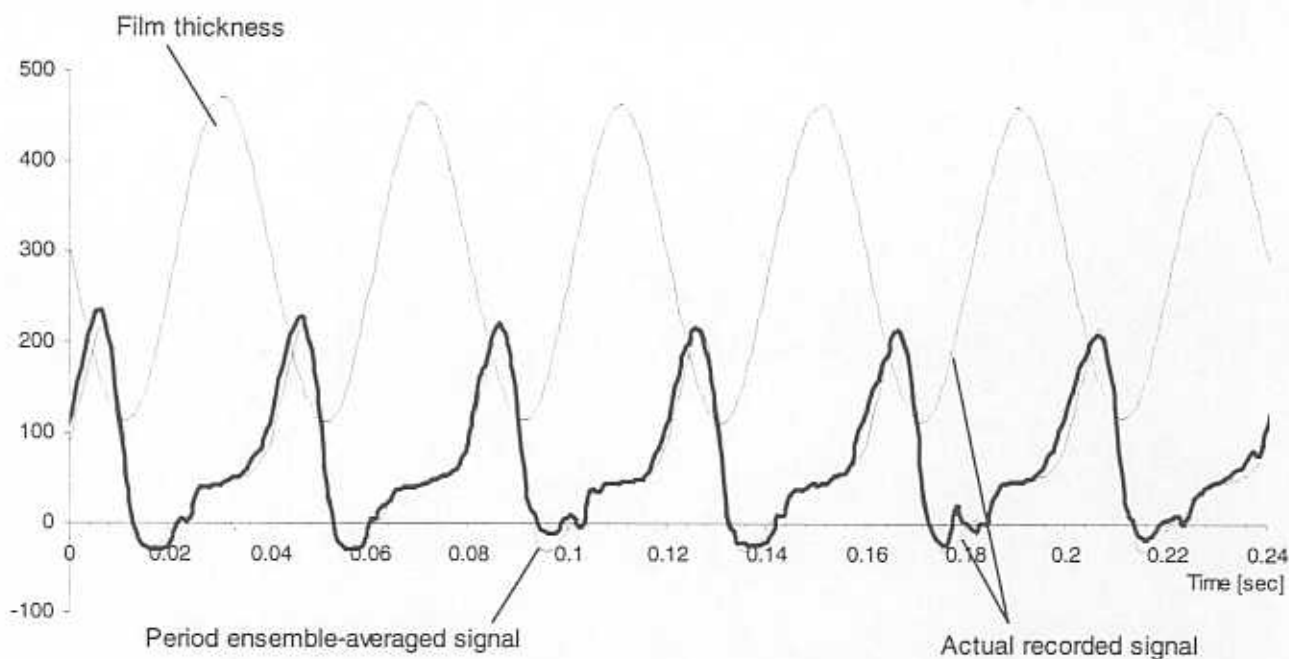
Figure 11. Film dynamic pressure (210°, Z₂) and period averaged pressure, and film thickness versus time for test at 1,500 rpm and 55 kPa (8 psi) gauge feed pressure. Period of motion =40 ms.
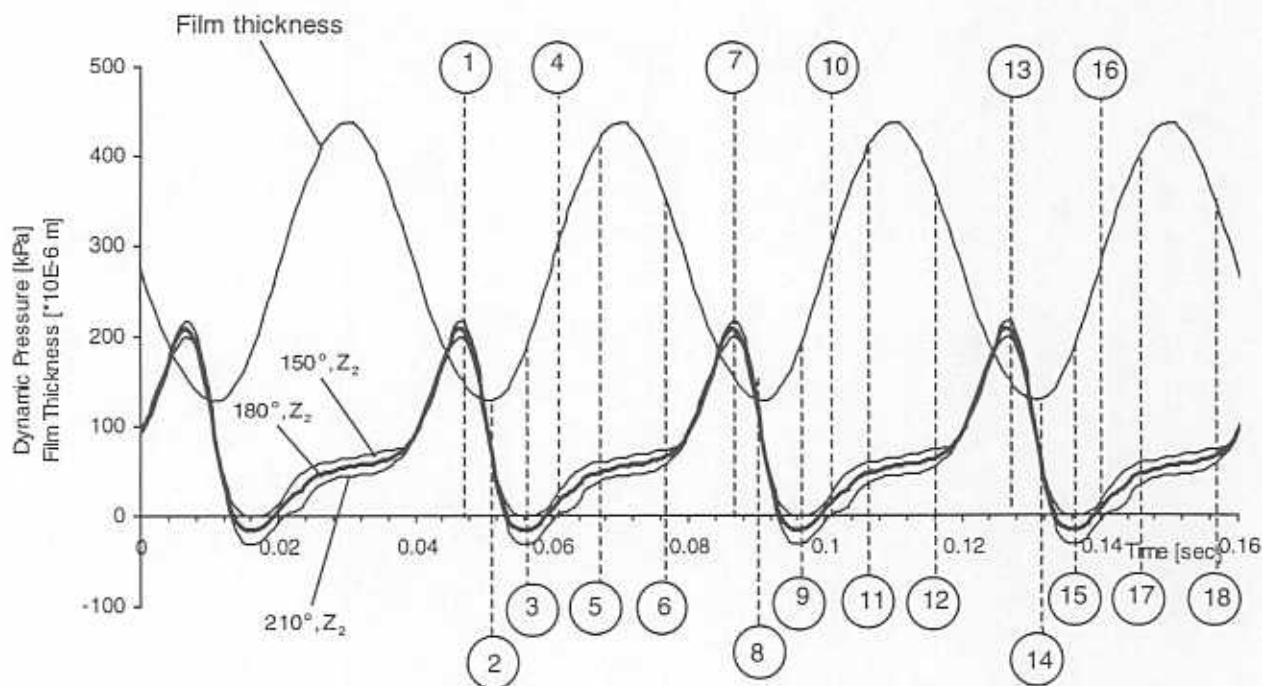
Figure 12. Period-average film pressures at (210°, Z₂), (150°, Z₂) and (180°, Z₂) and film thickness versus time for test at 1,500 rpm and 55 kPa (8 psig) gauge feed pressure. Numbered circles relate to photographs of flow depicted in Figure 13.

22
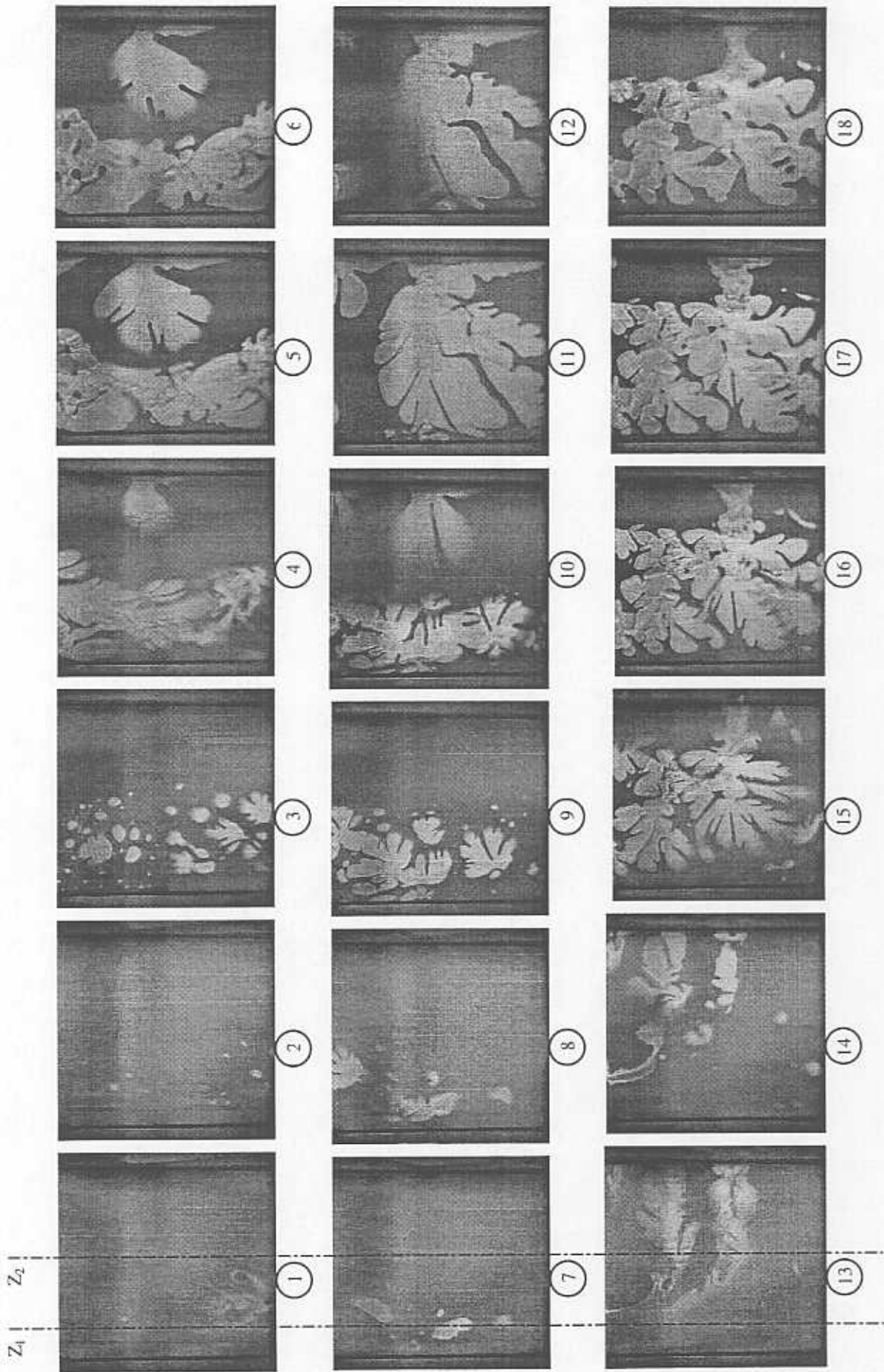
Figure 13. Photographs of flow field in SFD (30° span) at key instances of journal motion (see Figure 12). Frames in same column correspond to the same relative instant within a period of motion. Frames 1-6 correspond to 1st period, 7-12 to 2nd period, and 13-18 to 3rd period.

(a) t = 0.048 sec, P = 185 kPa at Z_2, h = 141μm

(b) t = 0.050 sec, P = 109 kPa at Z_2, h = 130μm (min. film)

(c) t = 0.052 sec, P = 32 kPa at Z_2, h = 132μm

(d) t = 0.054 sec, P = -10 kPa at Z_2, h = 148μm

(e) t = 0.056 sec, P = -16 kPa at Z_2, h = 181μm

(f) t = 0.056 sec, P = -16 kPa at Z_2, h = 181μm
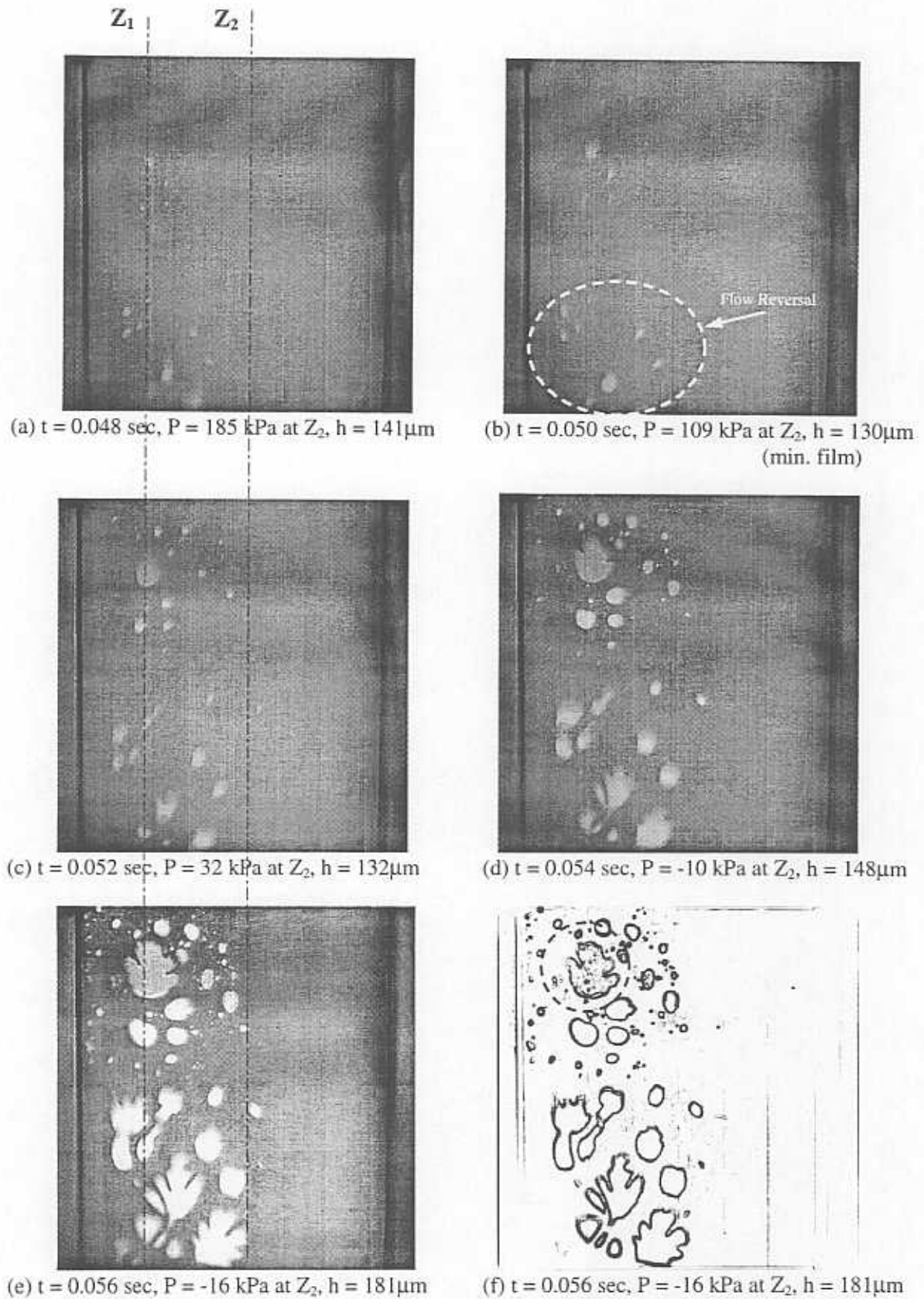
Figure 14. Series of flow images depicting bubble growth within lubricant film. Tests at 1,500 rpm and 55 kPa (8 psi) gauge feed pressure. Period of motion =40 ms.
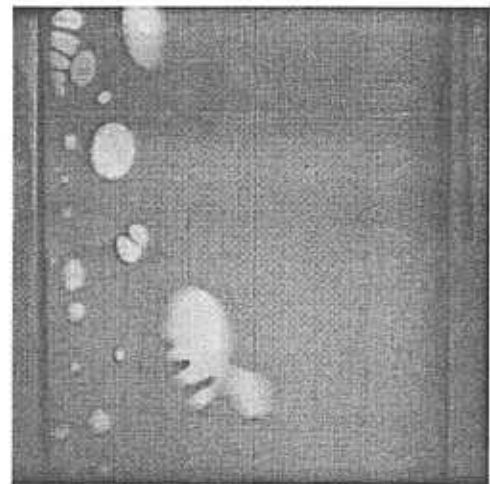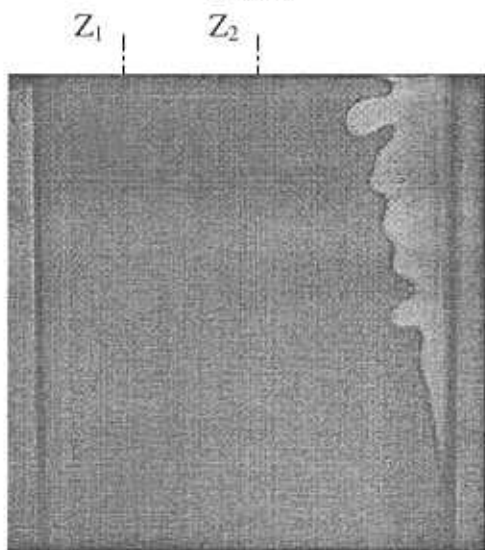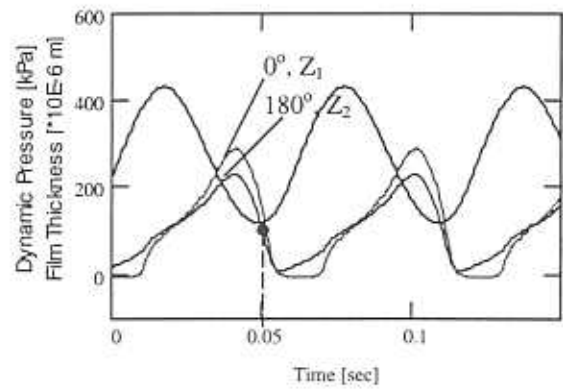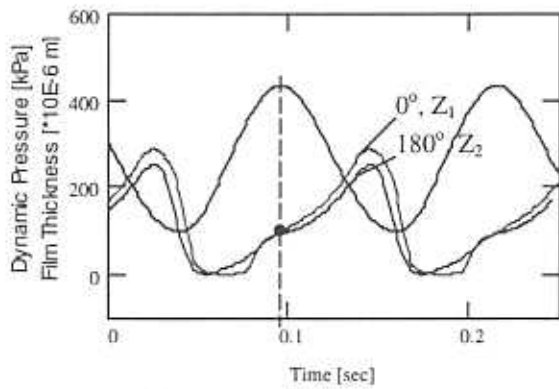
Figure 15. Film dynamic pressures and film thickness and flow photographs at
(a) 110 kPa/ 500 rpm, (b) 151 kPa/1,000 rpm.
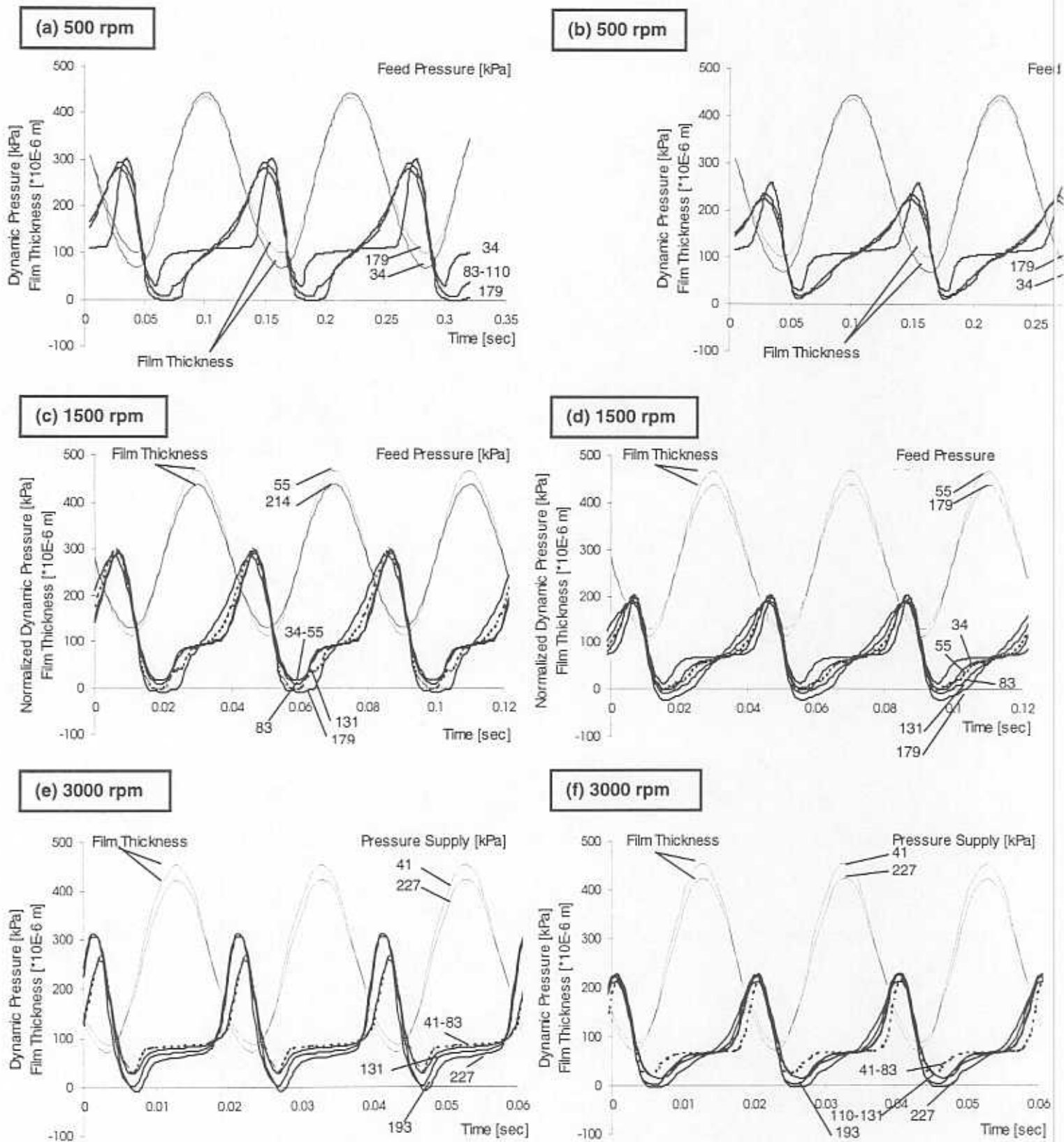
Figure 16. Film dynamic pressures and film thickness versus time for all tests. Feed pressure/speed varies. Left: Z_1 and right: Z_2 planes.

(a) t = 0.026 s
P = 3 kPa at Z_2
h = 140μm

(b) t = 0.028 s
P = 30 kPa at Z_2
h = 270μm

(c) t = 0.030 s
P = 50 kPa at Z_2
h = 380μm
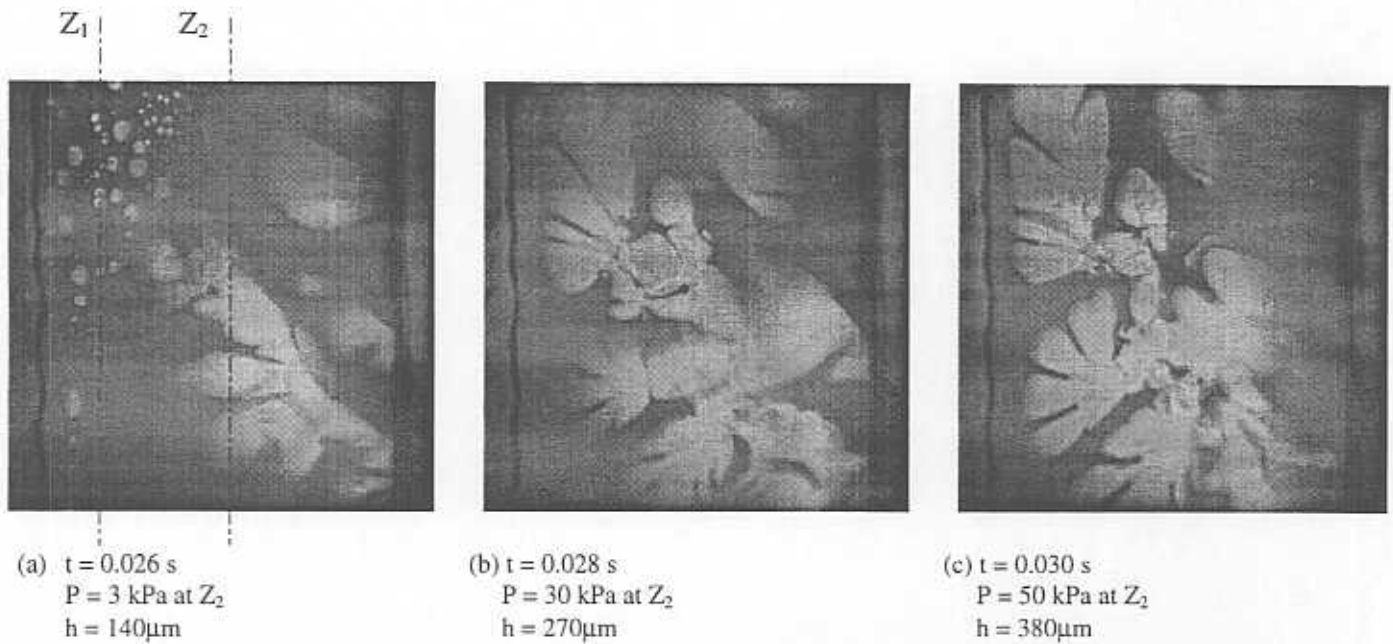
Figure 17. Photographs of flow field for a test at 1,500 rpm and feed pressure 193 kPa (28 psi).
Elapsed time for photographs is 2 ms (Period = 40 ms).
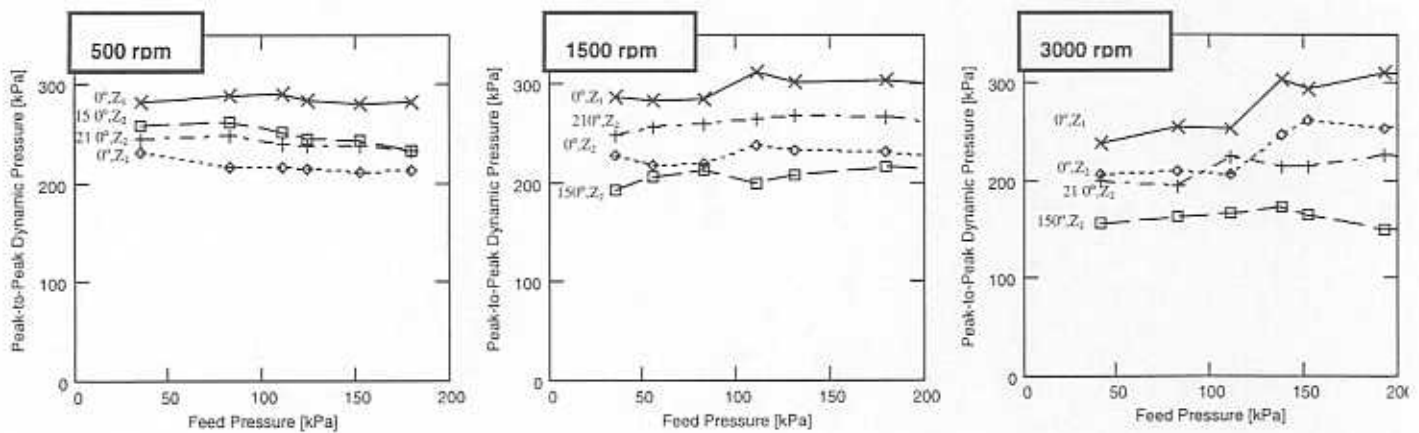
Figure 18. Peak-to-peak dynamic film pressures versus feed pressure for tests at
500, 1,500 and 3,000 rpm. Two axial locations of measurement.

27
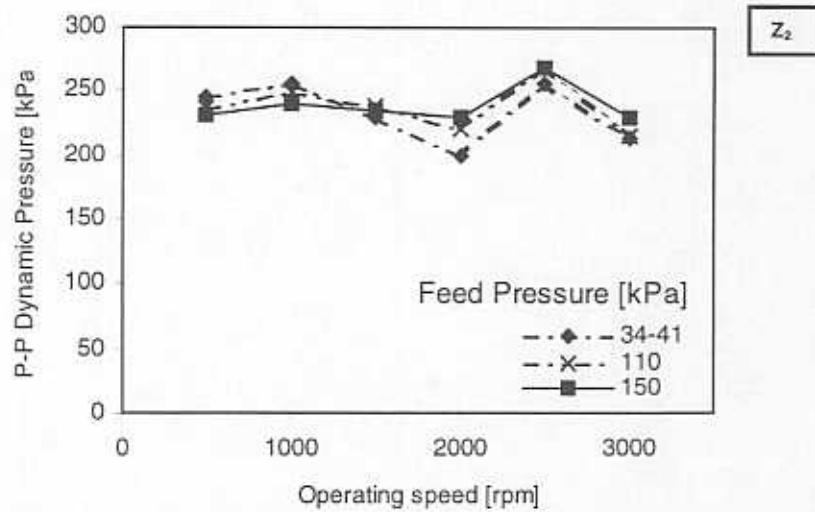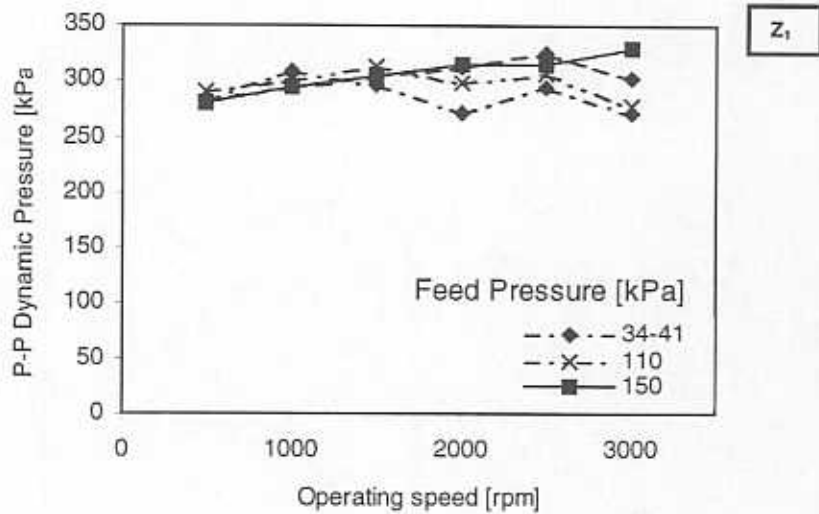
Figure 19. Peak-to-peak dynamic film pressures versus journal speed for range of feed pressures. Two axial locations of measurement noted.
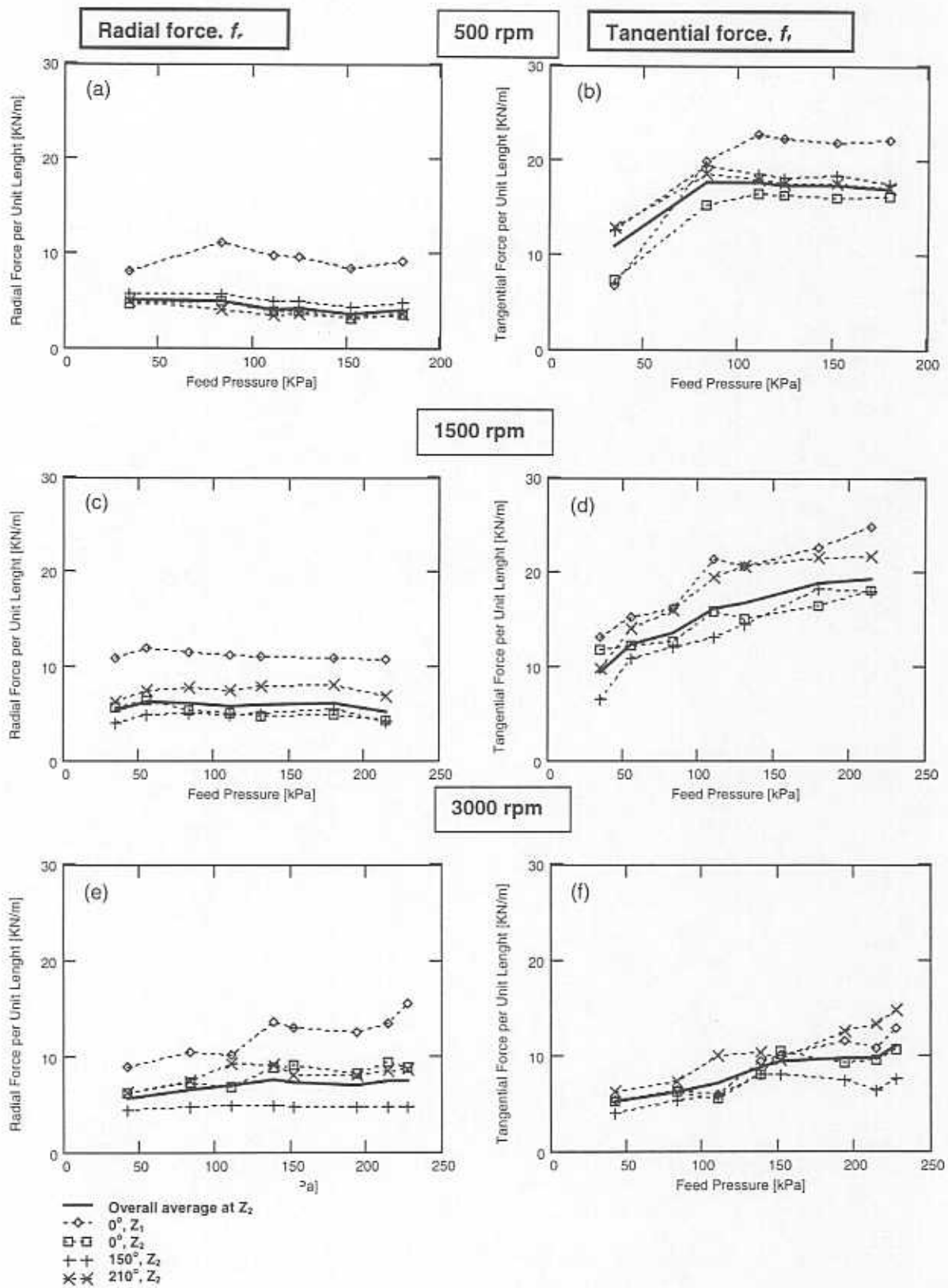
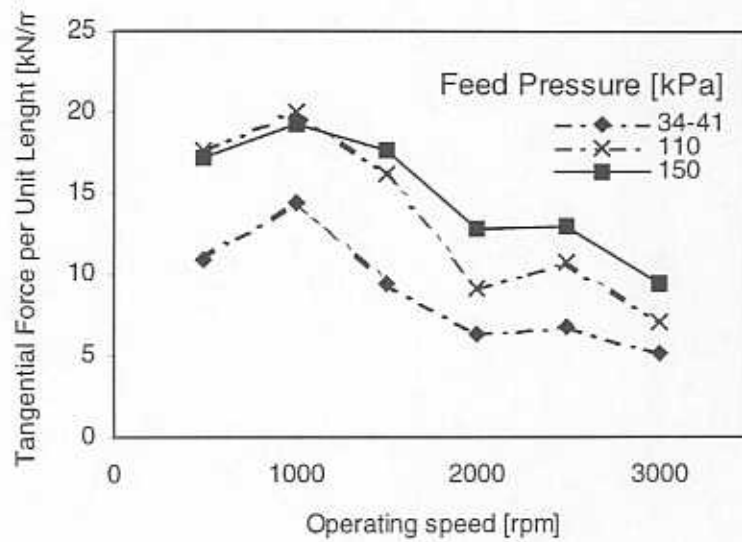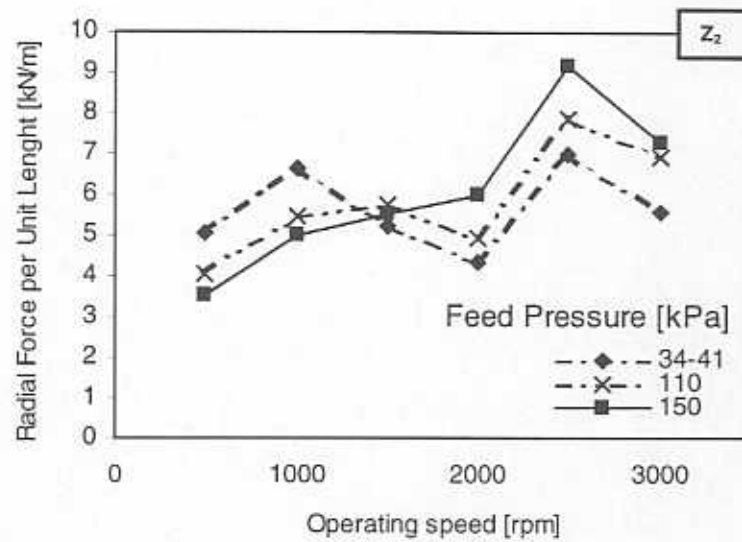**Figure 20. Estimated radial and tangential damper forces/unit length versus feed**

Figure 21. Estimated radial and tangential damper forces/unit length versus journal speed at the planes of measurement. (Z_2 plane)